J. Fluid Mech. (1994), *vol.* 277, *pp.* 381–407

Dissolution or growth of soluble spherical oscillating bubbles

By MARIOS M. FYRILLAS AND ANDREW J. SZERI

Department of Mechanical & Aerospace Engineering, University of California, Irvine, CA 92717-3975, USA

(Received 2 August 1993 and in revised form 20 April 1994)

A new theoretical formulation is presented for mass transport across the dynamic interface associated with a spherical bubble undergoing volume oscillations. As a consequence of the changing internal pressure of the bubble that accompanies volume oscillations, the concentration of the dissolved gas in the liquid at the interface undergoes large-amplitude oscillations. The convection–diffusion equations governing transport of dissolved gas in the liquid are written in Lagrangian coordinates to account for the moving domain. The Henry's law boundary condition is split into a constant and an oscillating part, yielding the *smooth* and the *oscillatory* problems respectively. The solution of the oscillatory problem is valid everywhere in the liquid but differs from zero only in a thin layer of the liquid in the neighbourhood of the bubble surface. The solution to the smooth problem is also valid everywhere in the liquid; it evolves via convection-enhanced diffusion on a slow timescale controlled by the Péclet number, assumed to be large. Both the oscillatory and smooth problems are treated by singular perturbation methods: the oscillatory problem by boundary-layer analysis, and the smooth problem by the method of multiple scales in time. Using this new formulation, expressions are developed for the concentration field outside a bubble undergoing arbitrary nonlinear periodic volume oscillations. In addition, the rate of growth or dissolution of the bubble is determined and compared with available experimental results. Finally, a new technique is described for computing periodically driven nonlinear bubble oscillations that depend on one or more physical parameters. This work extends a large body of previous work on rectified diffusion that has been restricted to the assumptions of infinitesimal bubble oscillations or of threshold conditions, or both. The new formulation represents the first self-consistent, analytical treatment of the depletion layer that accompanies nonlinear oscillating bubbles that grow via rectified diffusion.

1. Introduction

A bubble that would ordinarily dissolve in a liquid may increase in mass, rather than dissolve, if it undergoes volume oscillations in response to some perturbation. Previous analyses of the problem of the mass transport associated with an oscillating bubble have focused on the phenomenon of rectified diffusion, first identified by Blake (1949). In rectified diffusion, the normal process of dissolution of a gas bubble in a liquid may be reversed by sufficiently intense volume oscillations; hence a bubble which pulsates owing to the influence of an acoustic pressure field may grow if the amplitude of the pressure oscillations exceeds a certain *threshold* value. There are three factors that lead to this curious phenomenon. First, as the bubble volume changes,

so also does the internal pressure; this changes the concentration of dissolved gas in the liquid at the bubble interface, as determined by Henry's Law. Second, as the bubble undergoes volume oscillations, the surface area available for transport across the interface changes dramatically. Third, volume oscillations are accompanied by radial motion in the liquid that is characterized by a velocity field that decays as r^{-2}; this causes material points in the liquid separated by some radial distance to converge and diverge over the course of a bubble oscillation. As we shall establish, much of the concentration field is very nearly a material field as a consequence of the small diffusivity of gases in liquids. Hence any means by which material points in the liquid converge or diverge will have an important effect on whatever diffusive process may occur, through alternate steepening and shallowing of concentration gradients.

Past analyses of the mass transport across the dynamic interface associated with a bubble undergoing spherical oscillations have been restricted to infinitesimal radial oscillations of the bubble, or to threshold conditions where there is no net transport, or to both of these limitations. The reason for the restriction to the equilibrium problem of threshold conditions is that it was not known how to formulate the problem for the concentration field away from threshold conditions. The theoretical difficulty hinges on determination of the motion of the net flux of dissolved gas either away from a dissolving bubble or toward a growing bubble. In the latter case the zone of liquid in which the gas concentration is lowered as a consequence of net bubble growth has been referred to as the depletion layer by several authors. An additional challenging problem is to develop a rigorous means by which to deduce the influence of convection associated with the bubble volume oscillations on the diffusion of the net flux of dissolved gas. In the present paper we describe a way to resolve these difficulties which constitutes a new formulation of the problem.

A detailed review of some of the past work in this area was conducted by Plesset & Prosperetti (1977); therefore we will be brief in our comments on the work they describe. We provide a detailed comparison of our formulation with the others in § 5 after undertaking the analysis.

We begin with the paper of Blake (1949), in which there is an estimation of the net inflow of dissolved gas using a quasi-static solution of the diffusion problem in the liquid. Hsieh & Plesset (1961) studied the problem by assuming that the forcing acoustic pressure field, the bubble radius, and the concentration of gas in the liquid at the surface of the bubble all have (small-amplitude) sinusoidal dependence on time. Eller & Flynn (1965) removed the restriction to small sinusoidal oscillations in favour of a restriction to high-frequency oscillations and performed a boundary-layer analysis in Lagrangian coordinates first introduced by Plesset & Zwick (1952). This form of approximation is known as the thin-diffusion-layer approximation; it is uniformly valid in time only at threshold conditions. In other words, no provision is made for net flux of dissolved gas toward or away from the bubble.

In two papers Skinner (1970, 1972) treated the mass transport problem of an oscillating bubble using an ingenious decomposition of the concentration field. In the first paper, Skinner computed the forcing pressure threshold for rectified diffusion associated with a bubble undergoing small-amplitude sinusoidal radial oscillations. The equilibrium concentration field was computed via a double perturbation scheme that assumed (i) that the oscillations are small, and (ii) that the concentration gradients in the liquid are negligible outside a thin layer.

In the second paper, Skinner studied the problem of mass transport associated with an oscillating bubble away from threshold conditions. Two separate boundary layers

in the concentration field near the bubble surface were identified. The first (thinner) layer is associated with the time-dependent concentration of gas in the liquid at the surface of the bubble that arises according to Henry's law. The second (thicker) layer is associated with net flux of dissolved gas in the liquid. The two layers were handled by decomposing the concentration field into two parts. Skinner used the solution for the concentration field to examine the rate of growth of the average radius of a bubble undergoing small-amplitude sinusoidal oscillations.

More recently, Crum (1980) reports an extension to the threshold theory of Eller & Flynn, and experimental results of bubble growth rates away from threshold that far exceed the theoretical predictions of Eller & Flynn (or related theories). In addition, Crum finds that the addition of surface-active material to the bubble has an effect on bubble growth rates that is dramatically greater than can be accounted for by a simple modification of surface tension in the theory. Also observed were significant departures from the theoretical thresholds at super- or sub-saturated conditions in the far field.

Crum & Hansen (1982) and Church (1988) compare the various results for threshold acoustic pressure amplitude for growth of gas bubbles by rectified diffusion. Crum & Hansen generalize the analysis of Eller & Flynn to include more accurate perturbation results for the radial oscillations and damping. Church demonstrates graphically the sensitive dependence of the phenomenon of rectified diffusion on gas concentration in the far field.

Numerical solutions of the convection–diffusion equation for the dissolved gas in the liquid are reported by Kamath & Prosperetti (1990). These authors report that away from saturation conditions, the theory of Eller & Flynn tends to over-predict the threshold driving pressure amplitude for rectified diffusion, and under-predict the growth rates of bubbles at conditions that exceed threshold.

Finally, another possible approach to this class of problems is represented by the recent work of Fannjiang & Papanicolaou (1994) and references therein. These authors develop a general framework for homogenization of convection–diffusion equations valid for small diffusivities and for steady, spatially periodic flow fields in infinite domains. However, the mass transport problem of interest here includes an unsteady, spatially inhomogeneous (but not spatially periodic) velocity field and an extremely problematic boundary condition.

In summary, there appears to be an adequate theory for threshold conditions in a saturated liquid, but very little progress has been made on the non-equilibrium problem of nonlinear bubble growth or dissolution away from threshold conditions. The principal practical deficiency of the theory is the under-prediction of bubble growth rates at conditions that exceed threshold, especially for bubbles intentionally contaminated with surface-active materials as mentioned in Crum (1980, 1984). Even in the absence of consideration of the effects of surfactants, the growth or dissolution of nonlinearly oscillating bubbles has not been addressed owing to the difficulties mentioned above, i.e. a rigorous formulation of convection-enhanced diffusion, etc.

In the present paper, we treat the problem of a single bubble oscillating in a liquid of arbitrary saturation, i.e. away from threshold conditions. This work is part of an on-going project to understand the role of surfactants in gas transport across a dynamic interface. At this stage, we focus on developing the mathematical techniques required to solve convection–diffusion equations outside an oscillating bubble, together with complicated unsteady boundary conditions at the interface.

2. Formulation

In this section we formulate the mass transport problem and concentrate on the practical problem of large Péclet number. The differential equation governing the convection and diffusion of a dissolved gas in a liquid outside a spherically symmetric bubble is, in spherical polar coordinates,

$$\frac{\partial \tilde{C}}{\partial t} + \frac{R^2(t)\dot{R}(t)}{r^2}\frac{\partial \tilde{C}}{\partial r} = \frac{D}{r^2}\frac{\partial}{\partial r}\left(r^2\frac{\partial \tilde{C}}{\partial r}\right), \tag{2.1}$$

where $\tilde{C}$ is the mass fraction of gas dissolved in the liquid, $R^2(t)\dot{R}(t)/r^2$ is the radial velocity field in the liquid associated with the bubble oscillations, D is the diffusivity of the gas in the liquid, and the bubble radius R is a function of time t. Note that the velocity field in the liquid is time-dependent, spatially inhomogeneous and occurs in a domain with a moving boundary.

The dynamical equation for bubble oscillations is a nonlinear differential equation, such as the Rayleigh–Plesset equation, with derivation reviewed by Prosperetti (1984):

$$R\ddot{R} + \frac{3}{2}\dot{R}^2 = \frac{1}{\rho}\left(p_{Gi}\left(\frac{a}{R}\right)^{3\eta} + p_v(T_\infty) - p_s(t) - \frac{2\gamma}{R} - \frac{4\mu\dot{R}}{R}\right).$$

Although the results we develop in the present work apply irrespective of exactly which bubble dynamical equations are used, we have written the Rayleigh–Plesset equation in order to fix ideas and aid in non-dimensionalization. Here and in what follows, ρ is the density of the liquid, m_G is the mass of the gas in the bubble, M is the molecular weight of the gas, R_G is the universal gas constant, T_∞ is the temperature of the fluid, p_v is the vapour pressure, p_s is the pressure in the liquid, γ is the interfacial tension and μ is the viscosity of the liquid. The polytropic exponent η varies between the extremes of unity for an isothermal bubble and the ratio of specific heats c_p/c_v for an adiabatic bubble.

The boundary condition at the bubble surface is developed by application of Henry's law, which relates the concentration of a gas in a liquid to the partial pressure of the gas above the liquid; hence

$$\tilde{C}(r = R(t), t) = \frac{p_G}{k}.$$

Here, p_G is the partial pressure of the gas and k is the constant of Henry's law. For oscillations of a gas bubble with initial pressure equal to p_{Gi}, the surface boundary condition may be written

$$\tilde{C}(r = R(t), t) = \frac{p_{Gi}}{k}p_G^*(t), \tag{2.2}$$

where $p_G^*(t)$ is dimensionless. The bubble is assumed to be created in a fluid which initially has a uniform concentration of the gas C_∞. Hence the initial condition and the far-field conditions are

$$\tilde{C}(r, t = 0) = \tilde{C}(r \to \infty, t) = C_\infty. \tag{2.3}$$

The rate of transport of gas across the bubble interface is

$$\frac{\mathrm{d}m_G}{\mathrm{d}t} = 4\pi R^2 D\,\frac{\partial \tilde{C}(r = R(t), t)}{\partial r}.$$

The problem may be non-dimensionalized with respect to the following natural scales. As a lengthscale, we take a, the radius of the undisturbed bubble. The

timescale is Ω_0^{-1}, which is the inverse of the natural frequency of radial oscillations of the bubble about the undisturbed state. The pressure is made dimensionless using the pressure scale $\frac{1}{2}\rho a^2\Omega_0^2$. This leads to dimensionless parameters corresponding to the gas pressure in the undisturbed bubble,

$$p_{Gi}^* = \frac{3m_G R_G T_\infty}{2\pi M \rho a^5 \Omega_0^2} = \frac{2p_{Gi}}{\rho a^2 \Omega_0^2},$$

the Weber number *We*,

$$We = \frac{2\rho(a\Omega_0)^2 a}{\gamma},$$

the Reynolds number *Re*,

$$Re = \frac{\rho(a\Omega_0)a}{\mu},$$

and the dimensionless forcing pressure

$$p^*(\tau) = \frac{p_s(\tau\Omega_0^{-1}) - p_v(T_\infty)}{\frac{1}{2}\rho a^2\Omega_0^2}.$$

The convection–diffusion equation (2.1) is non-dimensionalized to read

$$\frac{\partial C}{\partial \tau} + \frac{x^2(\tau)x_\tau(\tau)}{\xi^2}\frac{\partial C}{\partial \xi} = \frac{1}{Pe}\frac{1}{\xi^2}\frac{\partial}{\partial \xi}\left(\xi^2\frac{\partial C}{\partial \xi}\right), \tag{2.4}$$

where ξ is the dimensionless radial coordinate, $x(\tau)$ is the dimensionless bubble radius, and the Péclet number is $Pe = a^2\Omega_0/D$. Next we non-dimensionalize the Henry's law boundary condition (2.2) to read

$$C(\xi = x(\tau), \tau) = \frac{p_{Gi}^*}{k^*}p_G^*(\tau) - C_\infty.$$

The dimensionless Henry's law constant is $k^* = 2k/\rho(a\Omega_0)^2$. Note that we have subtracted the concentration at infinity from the concentration field, i.e. $C = \tilde{C} - C_\infty$. Hence the initial and far-field conditions (2.3) become

$$C(\xi, \tau = 0) = C(\xi \to \infty, \tau) = 0.$$

Finally, for a motionless bubble, we have

$$p_{Gi}^* = p_0^* + \frac{8}{We},$$

from which we obtain an alternative expression of the boundary condition at the bubble surface

$$C(\xi = x(\tau), \tau) = \frac{p_0^*}{k^*}\left(1 + \frac{8}{p_0^* We}\right)p_G^*(\tau) - C_\infty. \tag{2.5}$$

The saturation concentration in the liquid separated from gas at pressure p_0^* by a plane boundary is $C_{sp} = p_0^*/k^*$. The saturation concentration in the liquid separated from gas within a spherical bubble of dimensionless radius $x = 1$ is

$$C_{sb} = C_{sp}\left(1 + \frac{8}{p_0^* We}\right) = \frac{p_{Gi}^*}{k^*}.$$

2.1. *Lagrangian formulation*

The principal analytical difficulties presented by the governing equations are the following. First, the boundary condition at the surface of the bubble (2.5) is applied at a time-dependent value of the radial coordinate $\xi = x(\tau)$; hence the problem is one with a moving boundary. Moreover, the boundary condition applied at the moving boundary is unsteady. The second observation is that the spatially inhomogeneous convection velocity can change sign, and is a nonlinear function of the bubble radius which evolves according to its own (nonlinear) ordinary differential equation. It is not possible to judge whether the convection tends to drive dissolved gas toward or away from the bubble. The goal of the present analysis is to refrain from specification of the bubble oscillation during development of the general theory in order that the concentration field and enhancement of transport may be studied for bubble oscillations that are as general as possible.

The first analytical difficulty, namely the moving boundary, can be eliminated by transforming the problem into Lagrangian coordinates; this is suggested by the observation that the bubble surface is a material surface. We assume the fluid outside the bubble is incompressible (at least for the purposes of solution of the convection–diffusion equation). Volume conservation and the particle paths one can obtain from the velocity field imply that the coordinate $\sigma = \frac{1}{3}(\xi^3 - x^3(\tau))$ has a constant value for a particle of fixed identity. In what follows, we shall work in the Lagrangian coordinates (σ, τ) rather than in the Eulerian coordinates (ξ, τ).

Equation (2.4) for the concentration field takes the form

$$\frac{\partial C}{\partial \tau} = \frac{1}{Pe}\frac{\partial}{\partial \sigma}\left(\left(3\sigma + x^3(\tau)\right)^{(4/3)}\frac{\partial C}{\partial \sigma}\right), \tag{2.6}$$

with boundary and initial conditions

$$\left.\begin{aligned} C(\sigma = 0, \tau) &= C_{sb}\, p_G^*(\tau) - C_\infty, \\ C(\sigma, \tau = 0) &= C(\sigma \to \infty, \tau) = 0. \end{aligned}\right\} \tag{2.7}$$

The equations now describe a field in a domain with a fixed boundary at the bubble surface.

In dimensionless, Lagrangian variables, the rate of transport is given by

$$\frac{\mathrm{d}m_G^*}{\mathrm{d}\tau} = \frac{3}{Pe}x^4\,\frac{\partial C(\sigma = 0, \tau)}{\partial \sigma}, \tag{2.8}$$

where m_G^* is m_G divided by the mass of liquid displaced by the undisturbed bubble.

2.2. *Splitting of the problem*

In the limit of infinite Pe, the concentration field is simply determined by the initial condition and the motion of the fluid particles outside the bubble; this is a consequence of the fact that (2.6) has the solution $C(\sigma)$ in that limit. However, the solution for large, but finite Pe is not a smooth perturbation of the solution for infinite Pe but a singular one. Physically, the reasons for this are as follows. when $Pe = \infty$, the concentration field is a material field, with C constant for each material point of fluid outside the bubble. When $1 \ll Pe < \infty$, however, the existence of diffusion means that C changes slowly for a material point of fluid, in response to the gradient in C with neighbouring material points. Of course, the gradient in C with neighbouring material points alternately steepens and shallows over a cycle of bubble oscillation. Hence there are two timescales that are important in the problem; the indications are

that a multiple-scales approach will be profitable. We refer the interested reader to the recent book by Hinch (1991) for an insightful discussion of this reasoning.

Another analytical difficulty is the time-dependent boundary condition (2.7). At large *Pe*, the concentration field will be characterized by oscillatory behaviour close to the bubble surface, due to the Henry's law boundary condition, and by slow diffusion further away from the bubble. To solve for the concentration field, it is profitable to split the problem into two parts. One part, the oscillatory problem, corresponds to the oscillatory part of the boundary condition, but as we shall see this part contributes nothing to the mass transport, asymptotically in time. The second part, the smooth problem, represents the constant part of the boundary condition which produces the same effect on the concentration in the far field as the full, time-dependent boundary condition. This constant boundary condition is not arbitrary but actually emerges from the solution of the oscillatory problem.

To begin the splitting, we define the average with respect to a convenient new nonlinear time $\hat{\tau}$

$$\hat{\tau}(\tau) \equiv \int_0^{\tau} x^4(\theta)\mathrm{d}\theta; \tag{2.9}$$

the average is

$$\langle f(\sigma,\tau)\rangle_{\hat{\tau}} \equiv \frac{1}{\hat{\tau}(T)}\int_0^{\hat{\tau}(T)} f(\sigma,\hat{\tau})\mathrm{d}\hat{\tau} = \frac{1}{\displaystyle\int_0^T x^4(\tau)\mathrm{d}\tau}\int_0^T f(\sigma,\tau)x^4(\tau)\mathrm{d}\tau,$$

where T is the dimensionless period of bubble oscillation. This somewhat peculiar averaging scheme will soon emerge as a clear manifestation of the spherical nature of the problem.

Using this average, we split the boundary condition at the surface of the bubble (2.7) as follows:

$$C(\sigma=0,\tau) = C_{sb}\,p_G^*(\tau) - C_\infty = C_{sb}\,\langle p_G^*(\tau)\rangle_{\hat{\tau}} - C_\infty + C_{sb}\left[\,p_G^*(\tau) - \langle p_G^*(\tau)\rangle_{\hat{\tau}}\right],$$

where the oscillating part is associated with the oscillatory problem and the constant part with the smooth problem. The *oscillatory problem* is therefore

$$\frac{\partial C_{osc}}{\partial\tau} = \frac{1}{Pe}\frac{\partial}{\partial\sigma}\left(\left(3\sigma + x^3(\tau)\right)^{(4/3)}\frac{\partial C_{osc}}{\partial\sigma}\right), \tag{2.10}$$

with boundary and initial conditions

$$\left.\begin{aligned} &C_{osc}(\sigma=0,\tau) = C_{sb}\left[\,p_G^*(\tau) - \langle p_G^*(\tau)\rangle_{\hat{\tau}}\right],\\ &C_{osc}(\sigma,\tau=0) = C_{osc}(\sigma\to\infty,\tau) = 0. \end{aligned}\right\} \tag{2.11}$$

The *smooth problem* is defined by

$$\frac{\partial C_{sm}}{\partial\tau} = \frac{1}{Pe}\frac{\partial}{\partial\sigma}\left(\left(3\sigma + x^3(\tau)\right)^{(4/3)}\frac{\partial C_{sm}}{\partial\sigma}\right), \tag{2.12}$$

with boundary and initial conditions

$$\left.\begin{aligned} &C_{sm}(\sigma=0,\tau) = C_{sb}\,\langle p_G^*(\tau)\rangle_{\hat{\tau}} - C_\infty,\\ &C_{sm}(\sigma,\tau=0) = C_{sm}(\sigma\to\infty,\tau) = 0. \end{aligned}\right\} \tag{2.13}$$

The sum of the solutions to the oscillatory and smooth problems is the solution to the

full problem, i.e. $C(\sigma,\tau) = C_{osc}(\sigma,\tau) + C_{sm}(\sigma,\tau)$. From equation (2.12) and boundary condition (2.13), it is straightforward to realize that (2.13) equal to zero gives the threshold criterion for rectified diffusion. We return to this point shortly.

The splitting just described closely parallels what one might do to solve for the motion in a fluid above an infinite flat plate that is moved horizontally in an impulsive fashion. Suppose that the plate is moved in an oscillatory manner with some non-zero mean velocity. As a consequence of the linear nature of the Navier–Stokes equations when restricted to the case of parallel flow in a domain of infinite extent, the problem is easily split in two. In one problem (Stokes' first problem, 1851) the flat plate moves at a uniform speed. In the second problem (Stokes' second problem) the flat plate oscillates with zero mean. In both cases the motion of the fluid is most easily understood by the diffusion of vorticity created by the no-slip boundary condition on the solid wall. We refer the interested reader to Kundu (1990) or to Leal (1992) for a discussion of these points. The main difference between Stokes' problems and the convection–diffusion problem pursued here is that we must resort to singular perturbation analyses in both oscillatory and smooth problems.

3. The oscillatory problem

Solution of the oscillatory problem provides the rationale for the non-intuitive averaging procedure used to split the problem in the previous section, as well as the threshold condition for rectified diffusion. However, the oscillatory solution contributes virtually nothing to the mass transport across the bubble surface even at conditions far removed from threshold. To solve the oscillatory problem, we re-scale the spatial coordinate σ by the square-root of the Péclet number. Hence we define $s = Pe^{1/2}\sigma$. The oscillatory equation (2.10) becomes

$$\frac{\partial C_{osc}}{\partial \tau} = \frac{\partial}{\partial s}\left(\left(3\frac{s}{Pe^{1/2}} + x^3(\tau)\right)^{(4/3)}\frac{\partial C_{osc}}{\partial s}\right).$$

In the limit of large Pe, this equation simplifies; to leading order, we have

$$\frac{\partial C^0_{osc}}{\partial \tau} = x^4(\tau)\frac{\partial^2 C^0_{osc}}{\partial s^2}, \tag{3.1}$$

where C^0_{osc} is the leading term in an expansion of the form

$$C_{osc}\left(\frac{s}{Pe^{1/2}},\tau\right) = C^0_{osc}(s,\tau) + \frac{1}{Pe^{1/2}}C^1_{osc}(s,\tau) + \cdots.$$

The leading-order problem may be solved by rescaling time as in (2.9) in order to transform to a canonical parabolic equation. This yields

$$\frac{\partial C^0_{osc}}{\partial \hat{\tau}} = \frac{\partial^2 C^0_{osc}}{\partial s^2}.$$

Hence, after application of techniques from singular perturbation theory and a nonlinear transformation of time, the leading-order solution of the oscillatory problem is identical to Stokes' second problem of flow near an oscillating flat plate. Eller & Flynn (1965) work out the details of the transient solution for the concentration field as an initial step in their analysis. However, they use a different boundary condition as we describe in § 5 below.

We compute the asymptotic solution $\bar{C}^0_{osc}$ (indicated by an overbar) via a Fourier

series approach, as follows. First, the boundary condition (2.11) is expanded as a Fourier series in the nonlinear time $\hat{\tau}$:

$$\bar{C}^0_{osc}(s=0,\hat{\tau}) = C_{sb}\left[\, p^*_G(\tau) - \langle p^*_G(\tau)\rangle_{\hat{\tau}}\right] = \sum_{m=1}^{\infty}\left[a_m \cos(\omega_m\hat{\tau}) + b_m \sin(\omega_m\hat{\tau})\right], \tag{3.2}$$

where

$$\omega_m = \frac{2m\pi}{\hat{\tau}(T)}.$$

It is of critical importance to note that there is no mean term in the Fourier expansion of the boundary condition in the nonlinear time by construction, because (2.11) implies

$$a_0 = \frac{1}{\hat{\tau}(T)}\int_0^{\hat{\tau}(T)} C^0_{osc}(s=0,\hat{\tau})\mathrm{d}\hat{\tau} = 0.$$

Next, we assume a (real) solution of the form

$$\bar{C}^0_{osc}(s,\hat{\tau}) = \sum_{m=-\infty,m\neq 0}^{\infty} A_m(s)\,\exp\left[\omega_m \mathrm{i}\,\hat{\tau}\right].$$

Term-by-term, one can solve to obtain the asymptotic concentration field for the oscillatory problem

$$\bar{C}^0_{osc}(s,\tau) = \sum_{m=1}^{\infty}\exp\left[-\left(\frac{\omega_m}{2}\right)^{1/2}s\right] \times\left\{a_m\cos\left[\omega_m\hat{\tau}-\left(\frac{\omega_m}{2}\right)^{1/2}s\right] + b_m\sin\left[\omega_m\hat{\tau}-\left(\frac{\omega_m}{2}\right)^{1/2}s\right]\right\}. \tag{3.3}$$

Each mode is heavily damped with distance s away from the bubble. For example, the amplitude of mode m is reduced to 1% when $s = 6.5/(\omega_m)^{(1/2)}$, i.e. when $\sigma = 6.5/(Pe\ \omega_m)^{(1/2)}$. Hence by requiring the mean term to be zero, the effect of the oscillatory boundary condition is localized to a small boundary-layer region close to the bubble. In order to expose the dependence of the boundary-layer thickness on the driving frequency we express ω_m and s in the original variables:

$$\left(\frac{\omega_m}{2}\right)^{1/2}s \equiv \left(\frac{m\pi a^2\Omega}{D}\frac{1}{\dfrac{1}{T}\displaystyle\int_0^T x^4(\theta)\mathrm{d}\theta}\right)^{1/2}\sigma,$$

where Ω is the driving frequency. The average of x^4 (known as the fourth moment) is large for oscillations that linger at large x. The parameters that tend to increase the boundary-layer thickness are low frequency, small bubbles, large diffusion coefficient and nonlinear bubble oscillations. In figure 1 we show the asymptotic solution of the oscillatory problem of the concentration field for $Pe = 1000$ and $x(\tau) = 1+0.1\sin(2\pi\tau)$.

The rate of mass transport (2.8) expressed in the nonlinear time $\hat{\tau}$ and scaled spatial coordinate s is

$$\frac{\mathrm{d}m^*_{G_{osc}}}{\mathrm{d}\hat{\tau}} = \frac{3}{Pe^{1/2}}\frac{\partial C_{osc}(s=0,\hat{\tau})}{\partial s}.$$

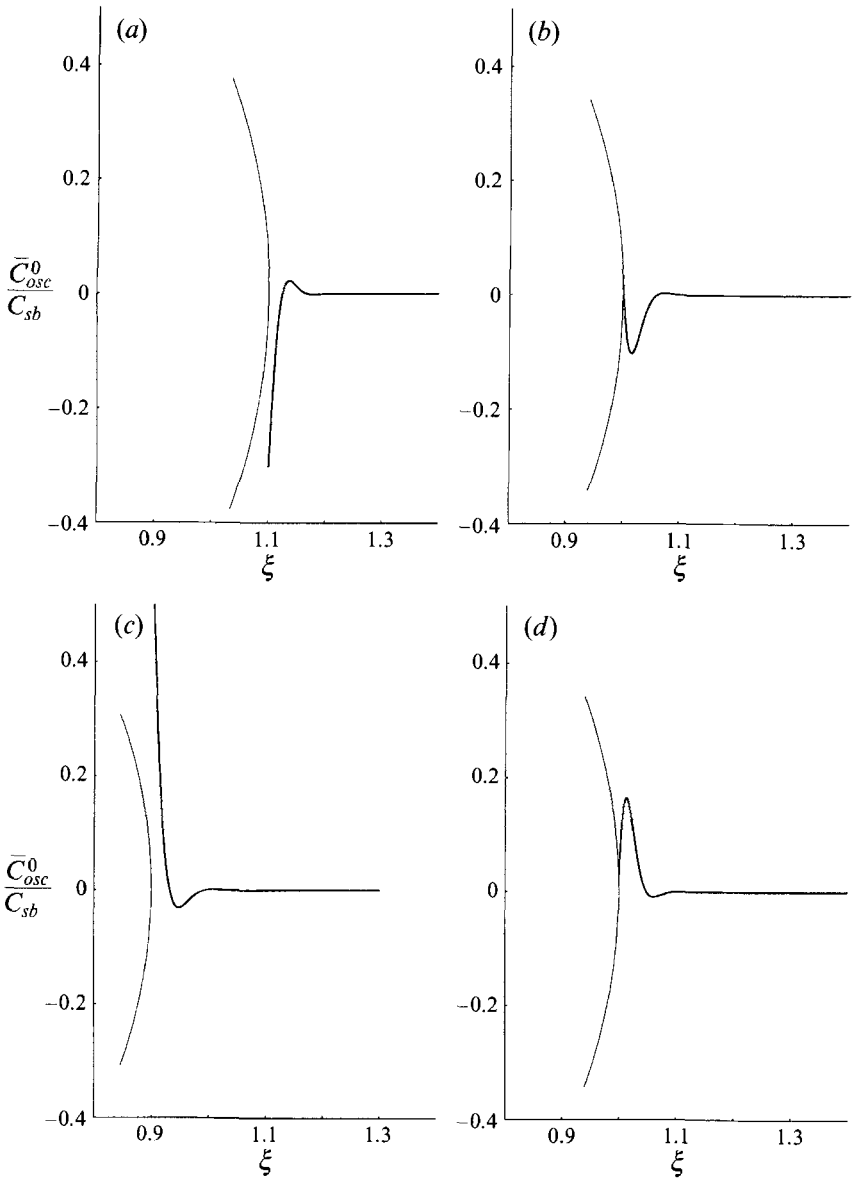

FIGURE 1. The asymptotic concentration profile for the oscillatory problem for $Pe = 1000$ and $x(\tau) = 1 + 0.1\sin(2\pi\tau)$, at (*a*) $\tau = T/4$, (*b*) $\tau = T/2$, (*c*) $\tau = 3T/4$ and (*d*) $\tau = T$. The plots show $\bar{C}^0_{osc}/C_{sb}$ versus the dimensionless Eulerian radial coordinate ξ. The circular arc shows the position of the bubble surface.

With the use of the asymptotic solution (3.3), it is a simple matter to determine that the associated mass transport over one period is zero. In Appendix A, we show that the asymptotic solution is reached very rapidly in a few periods of the bubble oscillation. Hence the mass transport associated with the transient in the oscillatory problem is negligible.

4. The smooth problem

It is in solving the smooth problem that we must develop a means by which to handle both convection-enhanced diffusion and the depletion layer associated with bubbles that grow by rectified diffusion. The smooth problem is characterized by slow convection-enhanced diffusion and by a steady boundary condition. Therefore, we introduce a second timescale $\lambda \equiv \tau/Pe = tD/a^2$, which captures the slow diffusive behaviour. Furthermore, we define for future use a second (conventional) time average with respect to τ over one period of bubble oscillation,

$$\langle f(\sigma,\tau)\rangle_\tau \equiv \frac{1}{T}\int_0^T f(\sigma,\tau)\mathrm{d}\tau. \tag{4.1}$$

Next we expand

$$C_{sm}(\sigma,\tau) = C^0_{sm}(\sigma,\lambda,\tau) + \frac{1}{Pe}C^1_{sm}(\sigma,\lambda,\tau) + \cdots.$$

Then, to zeroth order in the small parameter Pe^{-1}, we have the system

$$\frac{\partial C^0_{sm}}{\partial \tau} = 0, \tag{4.2}$$

with boundary and initial conditions

$$C^0_{sm}(\sigma = 0,\lambda,\tau) = C_{sb}\,\langle p^*_G(\tau)\rangle_{\hat{\tau}} - C_\infty,$$

$$C^0_{sm}(\sigma,\lambda = 0,\tau = 0) = C^0_{sm}(\sigma \to \infty,\lambda,\tau) = 0.$$

The solution to the zeroth-order problem (4.2) is simply $C^0_{sm}(\sigma,\lambda,\tau) = C^0_{sm}(\sigma,\lambda)$. However C^0_{sm} is further determined by the first-order problem:

$$\frac{\partial C^1_{sm}}{\partial \tau} = -\frac{\partial C^0_{sm}}{\partial \lambda} + \frac{\partial}{\partial \sigma}\left(\left(3\sigma + x^3(\tau)\right)^{(4/3)}\frac{\partial C^0_{sm}}{\partial \sigma}\right), \tag{4.3}$$

with boundary and initial conditions

$$C^1_{sm}(\sigma = 0,\lambda,\tau) = C^1_{sm}(\sigma,\lambda = 0,\tau = 0) = C^1_{sm}(\sigma \to \infty,\lambda,\tau) = 0.$$

We must ensure that there is no secular behaviour, lest the expansion become disordered as τ increases. Hence we force the right-hand side of the first-order problem (4.3) to have zero τ-average (defined in (4.1)); this leads to a second equation for C^0_{sm}

$$\frac{\partial C^0_{sm}}{\partial \lambda} = \frac{\partial}{\partial \sigma}\left(\langle\left(3\sigma + x^3(\tau)\right)^{(4/3)}\rangle_\tau \frac{\partial C^0_{sm}}{\partial \sigma}\right), \tag{4.4}$$

as a consequence of the critical simplification $C^0_{sm}(\sigma,\lambda,\tau) = C^0_{sm}(\sigma,\lambda)$. It is interesting to note that the two time averages we have defined, $\langle\cdot\rangle_{\hat{\tau}}$ and $\langle\cdot\rangle_\tau$, each has a strong physical motivation. The time average with respect to the nonlinear time has the property of extracting mean behaviour in Lagrangian spherical coordinates, whereas only the true time average can be used to distinguish secular behaviour.

The smooth problem has a very straightforward asymptotic solution $\bar{C}^0_{sm}(\sigma)$ (indicated by an overbar) in the limit $\lambda \to \infty$, obtained as follows. We set $\partial/\partial\lambda \equiv 0$ and integrate once with respect to σ. This yields

$$\frac{b}{\langle\left(3\sigma + x^3(\tau)\right)^{(4/3)}\rangle_\tau} = \frac{\mathrm{d}\bar{C}^0_{sm}}{\mathrm{d}\sigma},$$

where b is a constant to be determined. A definite integration from zero to ∞ yields

$$b\int_0^\infty \frac{\mathrm{d}\sigma}{\langle\left(3\sigma + x^3(\tau)\right)^{(4/3)}\rangle} = \bar{C}^0_{sm}(\sigma \to \infty) - \bar{C}^0_{sm}(\sigma = 0) = C_\infty - C_{sb}\langle p^*_G(\tau)\rangle_{\hat{\tau}}.$$

Therefore, the asymptotic solution to the smooth problem is

$$\bar{C}^0_{sm}(\sigma) = \left(C_{sb}\langle p^*_G(\tau)\rangle_{\hat{\tau}} - C_\infty\right)\left[1 - \frac{\displaystyle\int_0^\sigma \frac{\mathrm{d}\sigma}{\langle\left(3\sigma + x^3(\tau)\right)^{(4/3)}\rangle_\tau}}{\displaystyle\int_0^\infty \frac{\mathrm{d}\sigma}{\langle\left(3\sigma + x^3(\tau)\right)^{(4/3)}\rangle_\tau}}\right]. \tag{4.5}$$

We emphasize that this solution is valid, asymptotically in time, for any nonlinear periodic bubble oscillation. In figure 2 we show plots of the asymptotic, smooth concentration profile at various instants of time for $x(\tau) = 1 + 0.8\sin(2\pi\tau)$ and $p^*_G(\tau) = x^{-3.6}(\tau)$. In addition, $b = 0$ emerges clearly as the threshold condition for rectified diffusion.

The rate of mass transport (2.8) associated with the zeroth-order approximation of the smooth problem is

$$\frac{\mathrm{d}m^*_{G_{sm}}}{\mathrm{d}\lambda} = 3\langle x^4(\tau)\rangle_\tau \frac{\partial C^0_{sm}(\sigma = 0, \lambda)}{\partial\sigma}.$$

The asymptotic solution (4.5) gives an expression for the rate of mass transport

$$\frac{\mathrm{d}\bar{m}^*_{G_{sm}}(\lambda)}{\mathrm{d}\lambda} = -3\,\frac{\left[C_{sb}\,\langle p^*_G(\tau)\rangle_{\hat{\tau}} - C_\infty\right]}{\displaystyle\int_0^\infty \frac{\mathrm{d}\sigma}{\langle\left(3\sigma + x^3(\tau)\right)^{(4/3)}\rangle_\tau}}, \tag{4.6}$$

which is valid for any nonlinear periodic bubble oscillation. Because the denominator of (4.6) is always positive the threshold for rectified diffusion is therefore

$$C_{sb}\,\langle p^*_G(\tau)\rangle_{\hat{\tau}} - C_\infty = 0; \tag{4.7}$$

this agrees with the criterion developed by Eller & Flynn (1965). The growth rate of bubbles away from threshold conditions is close to the result of Eller & Flynn, except for large-amplitude oscillations.

The rate of mass transport associated with the transient in the smooth problem can be computed analytically only under the assumption of small oscillations as discussed in Appendix B. The mass transport associated with the transient solution of the smooth problem is quite significant at the initial stages. It reaches its asymptotic limit for $\lambda \approx 10$; this corresponds to $t \approx 10a^2/D$ if expressed in dimensional variables. For example, outside a bubble of radius 35μm, the rate of mass transport reaches its asymptotic value by $t = 5$ s. This is still a short time when compared to the experiments of Crum (1980) of 500 s duration.

5. Comparison with previous formulations

Now that we have completed our mathematical manalysis, it is useful to return to the work of previous researchers in this area. We shall focus on the analysis of Eller & Flynn (1965) as it is the basis for much of the theoretical work concerning rectified diffusion, including Eller (1969), Eller (1972), Crum (1980), Crum & Hansen (1982), and Church (1988). In each of these works, the underlying

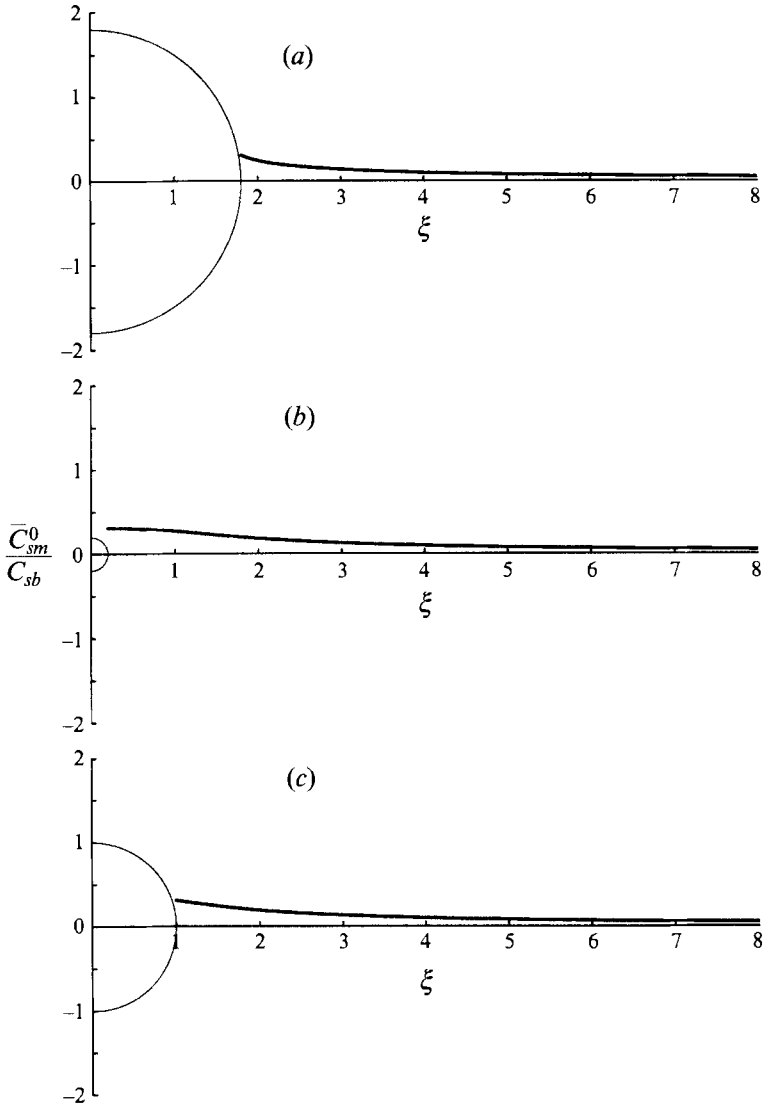

FIGURE 2. The asymptotic concentration profile for the smooth problem for the bubble oscillation $x(\tau) = 1 + 0.8\sin(2\pi\tau)$ and $p^*_G(\tau) = x^{-3.6}(\tau)$ at (*a*) $\tau = 0$, (*b*) $\tau = T/4$, and (*c*) $\tau = T/2$. The plots show $\bar{C}^0_{sm}/C_{sb}$ versus the dimensionless Eulerian radial coordinate ξ for the case $C_\infty = 0$. The circular arc shows the position of the bubble surface.

assumption is made that diffusion is of importance only in a thin layer near the surface of the bubble.

The thin-diffusion-layer approximation is exactly the same as the boundary-layer analysis we undertook to solve the oscillatory problem, with one exception. In the oscillatory problem, the boundary condition has zero average $\langle\cdot\rangle_{\hat{\tau}}$; this ensures that the oscillatory concentration field differs from zero only in a thin layer of thickness $O(Pe^{-1/2})$ near the bubble surface. In our solution of the oscillatory problem, this is the reason why the Fourier expansion of the boundary condition (3.2) has zero $\hat{\tau}$-mean.

In contrast, Eller & Flynn consider what we have called the oscillatory problem,

but they apply the full boundary condition, i.e. including the $\hat{\tau}$-average term in the Fourier expansion. In fact, when Eller & Flynn take their 'high-frequency limit', they simply replace the boundary condition by its $\hat{\tau}$-average! In other words, the high-frequency limit of Eller & Flynn is to solve what we call the oscillatory problem by applying what we use as the boundary condition of the smooth problem. This procedure, pursued by Eller & Flynn (and by others mentioned above), is valid only for short times, as pointed out in § 5 of their paper. The reason is that after some time has passed, the smooth boundary condition leads to a diffusion layer with thickness that grows like $\hat{\tau}^{1/2}$. Therefore the underlying assumption in the analysis eventually ceases to be valid. In the present paper we have defined unambiguously the splitting of the problem so that (i) the oscillating part of the boundary condition contributes (almost) nothing to the transport of gas and leads to a concentration field that differs from zero only in a thin layer of liquid near the bubble surface, for all time, and (ii) the steady part of the boundary condition is handled in a way that is uniformly valid in time and accounts for convection-enhanced diffusion.

6. Numerical results

Now we turn to numerical evaluation of the analytic expressions of (i) the threshold criterion for rectified diffusion and (ii) the rate of growth or dissolution of bubbles away from threshold conditions. A complete calculation of the rate of growth or dissolution of bubbles away from threshold conditions would, of course, have to account for slow changes in the periodic response of the bubble associated with its changing mass. However, close examination of the experimental results of Crum (1980) reveals that the rate of growth or dissolution is very nearly constant over several million periods of bubble oscillations. An exception occurs when Crum observes the emergence of obvious surface waves on larger (e.g. strongly forced 50μm) bubbles. This situation is clearly not addressed by the theory we have outlined. In summary, it would appear to be sufficient simply to examine the rate of growth of bubbles of various amplitudes under differing conditions.

The problem of computing the periodic response of a bubble to periodic variations in the background pressure has been approached via full numerical solution by Eller & Flynn (1965), by Eller (1969), and more recently by Church (1988) and Gaitan *et al.* (1992) using several different methods. In all cases except Eller (1969), the authors first computed then discarded the initial transient in order to obtain the asymptotic, periodic solution. The same is true in other areas of bubble research; Lauterborn (1976) also computed then discarded initial transients to obtain frequency-response curves for periodically driven bubbles. This proves to be an expensive undertaking, particularly when one wants to examine changes in the bubble oscillations over regions of multi-dimensional parameter space. Eller (1969) used a laborious shooting method to determine the initial conditions that lead to a periodic oscillation for a given set of parameter values. However, like the discarding of initial transients, this procedure also provides no information regarding why the oscillations change as one alters the parameter.

In view of these difficulties, many authors have assumed a (small-amplitude sinusoidal) form of the radius as a function of time, and used this as a basis for computing the required averages. These works include Hsieh & Plesset (1961), Eller (1969), Eller (1972), Crum (1980), Crum & Hansen (1982), and Nagiev & Khabeev (1985). For small amplitudes of pressure variation about the mean, these methods are satisfactory provided one is careful to avoid resonances.

We depart from previous work in what follows by using a new technique to compute asymptotic periodic bubble oscillations of arbitrary amplitude numerically, without proceeding through the transient. In order to accomplish this, we use a continuation algorithm to find the periodic bubble oscillation that is a global attractor at a new parameter value, by starting with an initial guess that is the converged solution at a nearby parameter value. The first task is to recast the system as an autonomous system of ordinary differential equations. This is easily done if one writes an auxiliary differential equation which has the periodic forcing as its global attractor. Then one simply couples the bubble oscillation to the driver. A suitable nonlinear driver sub-system is

$$\dot{x}_3 = x_3 + \theta\, x_4 - x_3\left(x_3^2 + x_4^2\right),$$
$$\dot{x}_4 = -\theta\, x_3 + x_4 - x_4\left(x_3^2 + x_4^2\right),$$

which has the asymptotic solution $x_3 = \sin(\theta t), x_4 = \cos(\theta t)$; the periodic driver motion is a normally hyperbolic limit cycle. Therefore, the stability of the periodic bubble oscillation will be characterized by the eigenvalues of the associated fixed point of the Poincaré (or period) map that derive from the bubble sub-system.

The numerical method we use is AUTO (Doedel 1986). The differential equations (in time) are discretized using an extremely efficient adaptive collocation procedure. In practice, this provides a very accurate and quick way to generate asymptotic periodic bubble oscillations directly as one varies a parameter. We remark that the method only works in the presence of damping in the problem, which makes the periodic solution an attractor, in the bubble sub-system. To begin the method, we simply set the parameter that controls the coupling between the driver and bubble sub-systems to zero. Hence the initial solution is just the (steady) equilibrium in the bubble sub-system $x(\tau) = 1$, and the periodic driving motion in the driver sub-system. Thereafter, changing the coupling parameter from zero results in a smooth development of the asymptotic bubble oscillation in response to the driving. Moreover, continuation is possible in any of the many parameters of the problem, e.g. equilibrium bubble radius, amplitude of the driving pressure oscillations, interfacial tension, liquid saturation, etc. Readers well-versed in nonlinear dynamics will note that the method we have outlined will detect a period-doubling bifurcation to a solution of the form $x(\tau) = x(\tau + 2T) \neq x(\tau + T)$. These solutions, which may occur at higher amplitudes of the forcing, are known to be of importance; see Lauterborn (1976), Smereka, Birnir & Banerjee (1987) and Kamath & Prosperetti (1989) for a discussion and examples. Note, however, that the quasi-periodic or chaotic motions described by these authors, as well as by Szeri & Leal (1991), cannot be approached by the technique just described.

6.1. *Nonlinear bubble dynamics*

The method just outlined may be applied directly to any suitable model of bubble dynamics. In view of the expected importance of resonances, as shown by the numerical results of Church (1988), and as a consequence of known inaccuracies of polytropic models near resonances, we make use of a more sophisticated non-polytropic bubble model. This model, like the polytropic models, assumes that the pressure field within the bubble is uniform. However a spatially non-uniform temperature field is allowed. This requires solution of the energy equation for the gas within the bubble, which is a partial differential equation. We shall use the four-term Galerkin formulation of Kamath & Prosperetti (1989). Hence, to the bubble

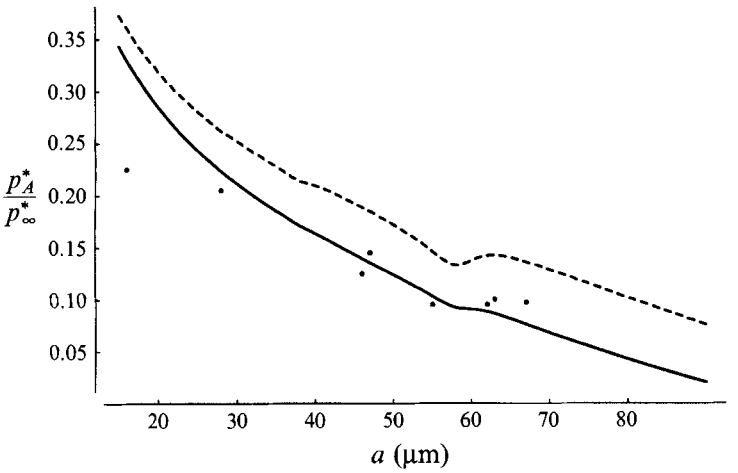

FIGURE 3. The ratio of the threshold pressure amplitude for rectified diffusion to the steady part of the background pressure versus equilibrium bubble radius. The bubbles are driven at a frequency of 26.6 kHz, and the interfacial tension is 73 dynes cm^{-1}. The dashed curve is (4.7) for saturated liquid (as reported by Eller 1969), the solid curve is (4.7) for a saturation of 101.5 % (a correction suggested by Church 1988), the points are the experimental data of Eller (1969).

sub-system and driver sub-system, we append four ordinary differential equations for the amplitude coefficients of the Galerkin expansion of the temperature field. The pressure inside the bubble is given explicitly by an equation based on constant mass of gas within the bubble. These equations are given in the appendix of the paper by Kamath & Prosperetti (1989). The bubble sub-system consists of a second-order ordinary differential equation which we transform into a first-order system, and use the same scales as before to non-dimensionalize; this yields

$$\frac{\mathrm{d}x_1}{\mathrm{d}\tau} = x_2$$

and

$$\frac{\mathrm{d}x_2}{\mathrm{d}\tau} = \left[3\,x_2^2\left(\frac{x_2}{3\,c^*}-1\right)+\left(1+\frac{x_2}{c^*}\right)(p_B^*-p^*) + \frac{x_1}{c^*}\left(\frac{8\,x_2}{We\,x_1^2}+\frac{8\,x_2^2}{Re\,x_1^2}-p_{Gi}^*\,\frac{\mathrm{d}p_G^*(\tau)}{\mathrm{d}\tau}\right)\right]\left[2\left(1-\frac{x_2}{c^*}\right)x_1+\frac{8}{Re\,c^*}\right]^{-1},$$

$$p_B^* = p_{Gi}^*\,p_G^*(\tau)-\frac{8}{We\,x_1}-\frac{8\,x_2}{Re\,x_1},$$

$$p^* = p_\infty^*\left[1-\frac{p_A^*\left((1/\Omega_0)[\tau+(x_1/c^*)]\right)}{p_\infty^*}\right],$$

and the dimensionless sound speed is $c^* = c/(a\Omega_0)$.

6.2. *Threshold criterion*

In figures 3 and 4 we show plots of the threshold criterion for rectified diffusion (4.7), together with some experimental points, due to Eller (1969) and Crum (1980) respectively. The physical parameters are the threshold ratio of the amplitude of pressure oscillations with respect to the background pressure versus the equilibrium

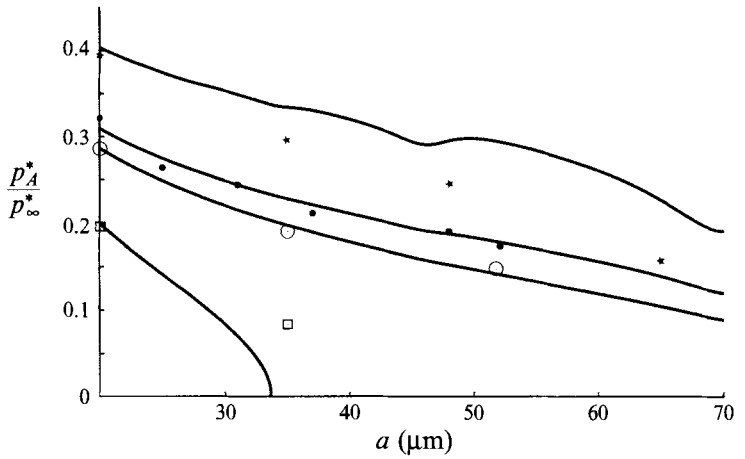

FIGURE 4. The ratio of the threshold pressure amplitude for rectified diffusion to the steady part of the background pressure versus equilibrium bubble radius for different far-field concentrations of gas in the liquid. The solid curves are (4.7), with $C_{sp}/C_\infty = 0.95$ (uppermost), 1.00, 1.01, and 1.04 (bottom). The points are the experimental data of Crum (1980) at the same conditions. The bubbles are driven at a frequency of 22.1 kHz and the interfacial tension is 68 dynes cm^{-1}.

bubble radius. The curves in the figures are computed as follows. We begin the continuation algorithm at the trivial (normally hyperbolic) periodic attractor in which the driver sub-system is completely decoupled from the bubble sub-system. Thereafter, the coupling parameter, which corresponds physically to the amplitude of background pressure variations, is increased slowly from zero. While this is happening, we monitor the value of the *threshold function*, the left-hand side of (4.7). As the pressure amplitude increases, yielding bubble oscillations of larger and larger amplitude, the threshold function smoothly passes through zero. We capture the exact value of the pressure amplitude at which the threshold function yields zero. In this way the threshold pressure amplitude is obtained for a bubble of a single equilibrium radius, without computing any transients.

From this first point, we use continuation to trace out the remainder of the threshold curve by switching tactics. The parameter corresponding to the value of the threshold function is held constant, while continuation in a takes place. An additional free parameter is required; this is met by the amplitude of pressure variations. As one can see from figures 3 and 4, the threshold pressure amplitude generally decreases with increasing equilibrium bubble radius.

Note that even with the improvements of the theory we have put forward in the present paper, including a much more sophisticated means for determination of nonlinear bubble oscillations, the problem remains that the threshold condition is accurate only near saturation. In other words, the threshold amplitude of background oscillations is in error, compared with the experiments shown in figures 3 and 4, at over-and under-saturated conditions. At saturations of 1 and 1.01, the threshold results agree quite well with the experimental data of Crum. The agreement between theory and the experimental data of Eller (1969), shown in figure 3, is not as good unless one takes as 101.5% as the saturation of the liquid. This correction is suggested by Church (1988). While the errors may in part be due to experimental difficulties, these results may also indicate the need to account for the physical effects of surfactants on the gas transport across the dynamic interface.

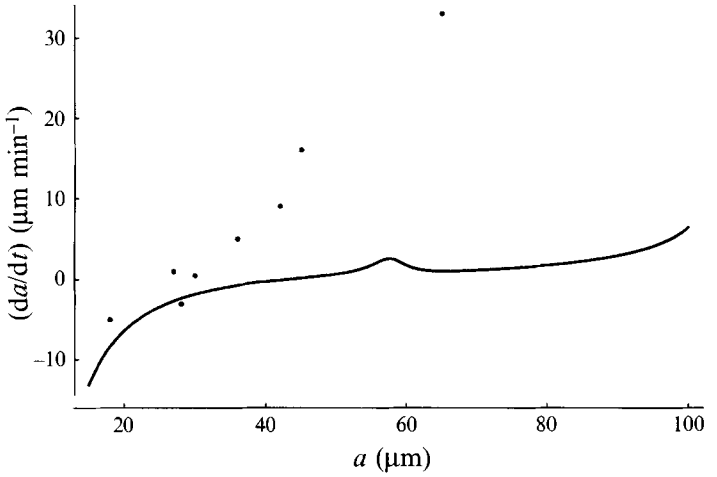

FIGURE 5. The rate of bubble growth in μm per minute versus equilibrium bubble radius in μm. The bubbles are forced at a pressure amplitude of 0.2 bar. The solid curve corresponds to (6.1), the points correspond to the experimental data of Eller (1969). The diffusivity of the gas in the liquid is 2.0×10^{-5} cm^2 s^{-1}. The bubbles are driven at a frequency of 26.6 kHz, and the interfacial tension is 73 dynes cm^{-1}.

6.3. *Rate of growth of bubbles away from threshold conditions*

Finally, we turn to an investigation of the rate of growth of bubbles away from threshold conditions. Following Eller (1969), the rate of growth of the equilibrium bubble radius is related to the mass transfer (given by (4.6)) as follows:

$$\begin{aligned}\frac{\mathrm{d}a}{\mathrm{d}t} &= a\,\Omega_0 \frac{R_G\,T_\infty \rho}{3\,M\,p_0}\frac{1}{Pe}\left(1+\frac{16}{3\,We\,p_0^*}\right)^{-1}\frac{\mathrm{d}m^*_{G_{sm}}}{\mathrm{d}\lambda}\\ &= a\,\Omega_0 \frac{R_G\,T_\infty \rho}{M\,p_0}\frac{1}{Pe}\left(1+\frac{16}{3\,We\,p_0^*}\right)^{-1}\frac{\left(C_\infty - C_{sb}\langle p^*_G(\tau)\rangle_{\hat{\tau}}\right)}{\displaystyle\int_0^\infty \frac{\mathrm{d}\sigma}{\langle\left(3\sigma + x^3(\tau)\right)^{(4/3)}\rangle_\tau}}.\end{aligned} \tag{6.1}$$

In figure 5 we show a plot of the rate of bubble growth versus equilibrium bubble radius, for bubbles forced by a background pressure field oscillating at an amplitude of 0.2 bar. Also included in the figure are the experimental points of Eller (1969). The general trend is for larger bubbles (in terms of equilibrium radius) to grow faster.

The slight bump at a just less than 60μm corresponds to a resonance in the bubble dynamical equations. This may be seen in the bubble response curve in figure 6. As the measure of the solution on the vertical axis, we have taken the maximum bubble radius over the periodic attractor. On the horizontal axis is the equilibrium bubble radius. For reference, in figure 7 we show several bubble time traces for various equilibrium bubble radii in figure 6.

One can observe that the bubble growth rates predicted theoretically by the methods outlined above, and plotted as the solid curve in figure 5 are of the same order as the experimental results. The predictions are quite good for smaller bubbles, but for larger bubbles the growth rates are quite seriously under-predicted. Contrary to the polytropic model (appendix C) the effect of resonances is ruled out as the reason for the poor agreement between theory and experiment. It would appear that the speculations of Crum (1980) and Church (1988) on the importance of surfactants

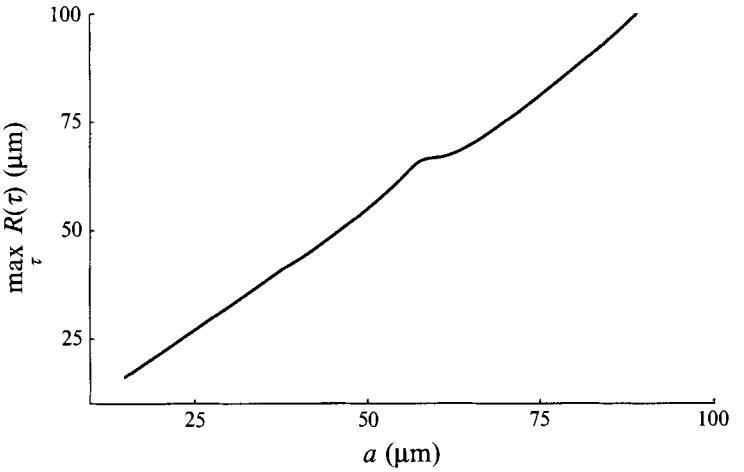

FIGURE 6. A bifurcation diagram or response curve. On the vertical axis, as a measure of the solution, we take the maximum bubble radius in μm over the period of oscillation. On the horizontal axis is the equilibrium bubble radius. The bubble oscillations are everywhere stable. The bubbles are driven at a frequency of 26.6 kHz, and the interfacial tension is 73 dynes cm^{-1}.

even in relatively clean laboratory situations cannot be overlooked in a complete description of the phenomenon of rectified diffusion.

7. Conclusions

We have presented a new formulation and solution of the problem of mass transport across the dynamic interface of a soluble spherical gas bubble undergoing volume oscillations in a liquid. The validity of the methods employed depends on the Péclet number being large, for then the timescale associated with diffusion of dissolved gas through the liquid is very much longer than the timescale associated with convection of dissolved gas by the radial velocity in the liquid arising from bubble oscillations. This approach is a departure from previous theoretical analyses of the problem, in which either infinitesimal bubble oscillations or threshold conditions (or both) were assumed. The principal theoretical barriers overcome in this work are (i) how to formulate the problem for the depletion layer outside a bubble that is growing via rectified diffusion (or the excess layer outside a dissolving bubble), (ii) how to handle convection-enhanced diffusion of dissolved gas in the liquid, where the motion is driven by the bubble oscillations, and (iii) how to formulate a problem for the time-dependent part of the Henry's law boundary condition that yields a solution that differs from zero only in a thin layer of liquid near the surface of the bubble, for all time.

To accomplish these advances, we split the convection–diffusion problem into two parts: the oscillatory problem and the smooth problem. The splitting corresponds in a certain sense we made specific to Stokes' first problem of the impulsive motion of an infinite flat plate and to Stokes' second problem of an oscillating infinite flat plate. The solutions to the oscillatory and smooth problems are valid everywhere in the liquid. The solution of the oscillatory problem is characterized by a boundary layer in the concentration field of thickness controlled by the Péclet number. The oscillatory concentration field accounts for the unsteady part of the boundary condition, but quickly approaches zero as one moves away from the bubble. The solution of the

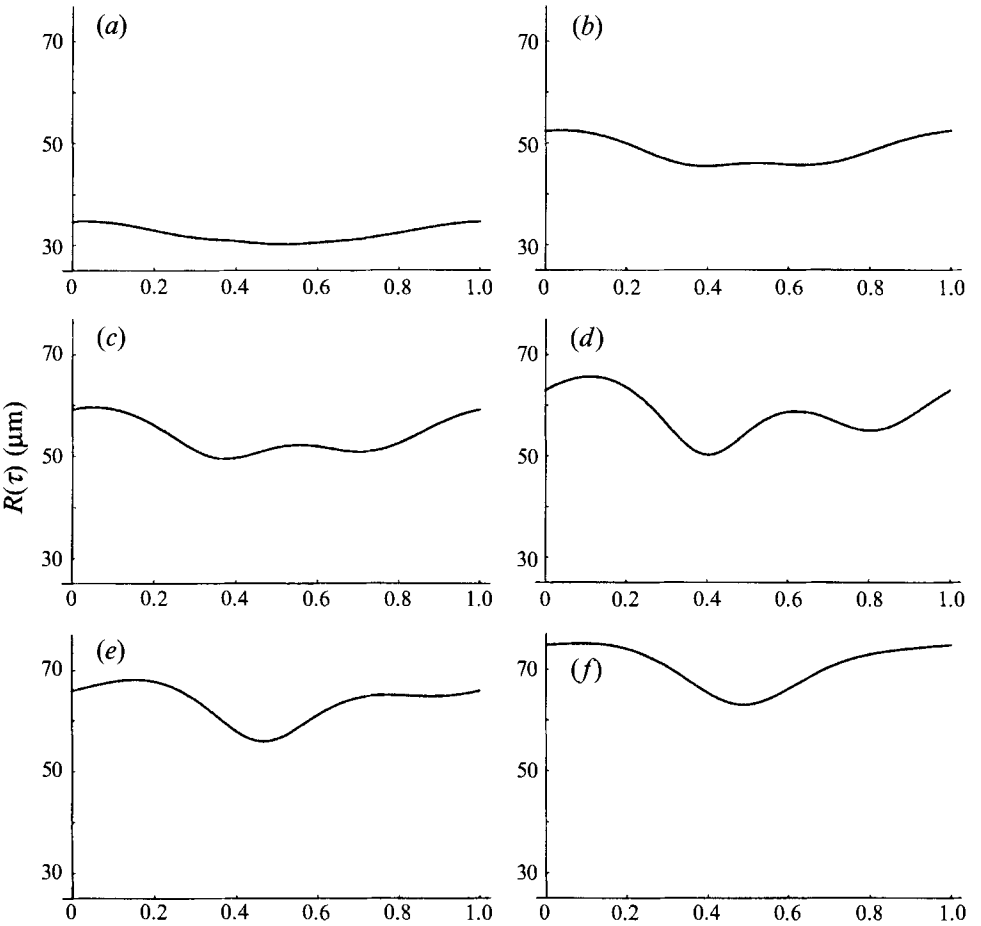

FIGURE 7. Time traces of the bubble response at various points along the branch indicated in figure 6. The plots show the bubble radius in μm versus dimensionless time. The equilibrium radii are (*a*) 32, (*b*) 48, (*c*) 53.4, (*d*) 57.4, (*e*) 62.9, and (*f*) 70 μm.

smooth problem accounts for the steady or average part of the boundary condition, as well as the net flux of dissolved gas toward or away from the oscillating bubble. As a consequence of the small diffusivity of gases in liquids, the smooth problem is efficiently treated using the method of multiple scales in time, with evolution on a slow timescale controlled by the Péclet number superposed on motion on the fast timescale associated with bubble oscillations. Unlike the work of previous authors described above, we need assume neither small-amplitude sinusoidal oscillations nor threshold conditions to solve for the concentration field using the new formulation.

Even with the progress reported here on the formulation and solution of the problem of mass transport across a dynamic interface, it seems clear after comparison with experimental results that some physics remains unaccounted for. Although the theory and experiment agree quite well for small bubbles that grow slowly in saturated liquids, the prevalence of large growth rates for strongly forced bubbles remains elusive. It would appear that a likely candidate for the remaining physics that ought to be included in a complete theory is the modification of the gas transport across the bubble surface due to the (ubiquitous) presence of surface active materials.

A. J. S. would like to acknowledge the support of the Office of Naval Research under the Young Investigator Program. The authors wish to thank Professor Eusebius Doedel for providing a copy of the software AUTO, and Professors Andrea Prosperetti and Howard Stone for assistance with several references. In addition, the authors thank a referee for emphasizing the inaccuracy of polytropic bubble models near resonance; this motivated the use of the non-polytropic model in the numerical results.

Appendix A. Transients in the oscillatory problem

Eller & Flynn (1965) work out the details of the transient solution to the oscillatory problem (3.1) for the concentration field given any boundary condition at $s = 0$,

$$C^0_{osc} = \frac{s}{2\pi^{1/2}} \int_0^{\hat{\tau}} \frac{1}{\theta^{3/2}} \exp\left(-\frac{s^2}{4\theta}\right) C^0_{osc}(s = 0, \hat{\tau} - \theta) \mathrm{d}\theta, \tag{A 1}$$

as an initial step in their analysis. As we have reported, the mass transport associated with the oscillatory problem is zero, after the decay of initial transients. This leads naturally to the question: how quickly does the mass transport associated with the transient solution of the oscillatory problem go to zero?

In order to determine this, we compute the mass transport obtained from the transient solution (A 1). After some manipulation we find

$$m^*_{G_{osc}}(\hat{\tau}) - m^*_{G_{osc}}(0) = \frac{3}{Pe^{1/2}} \int_0^{\hat{\tau}} \frac{C^0_{osc}(s = 0, \hat{\tau} - \theta)}{(\theta\pi)^{1/2}} \mathrm{d}\theta.$$

Next we make use of the Fourier expansion of the boundary condition (3.2), to obtain the change in bubble mass due to the transient part of the oscillatory problem

$$\begin{aligned} m^*_{G_{osc}}(\hat{\tau}) - m^*_{G_{osc}}(0) = \frac{3}{Pe^{1/2}} \sum_{m=1}^{\infty} \left(\frac{2}{\omega_m}\right)^{1/2} \\ \times \left\{ \left(b_m \, \mathrm{S}\left[\left(\frac{2\,\omega_m \hat{\tau}}{\pi}\right)^{1/2}\right] - a_m \, \mathrm{C}\left[\left(\frac{2\,\omega_m \hat{\tau}}{\pi}\right)^{1/2}\right] \right) \cos\left[\omega_m \hat{\tau}\right] \right. \\ \left. - \left(a_m \, \mathrm{S}\left[\left(\frac{2\,\omega_m \hat{\tau}}{\pi}\right)^{1/2}\right] + b_m \, \mathrm{C}\left[\left(\frac{2\,\omega_m \hat{\tau}}{\pi}\right)^{1/2}\right] \right) \sin\left[\omega_m \hat{\tau}\right] \right\}, \end{aligned}$$

where $\mathrm{S}[x]$ and $\mathrm{C}[x]$ are the sine and cosine Fresnel integrals respectively. These functions reach their asymptotic values of $1/2$ in a few periods of the bubble oscillation. Thereafter each term in the Fourier expansion corresponds to an oscillation with zero mean. We conclude that the oscillatory problem contributes very little to the transport across the bubble surface, and then only in the first few periods of oscillation.

Appendix B. Transients in the smooth problem

We were able to determine in § 4 the asymptotic concentration field associated with the smooth problem for any nonlinear periodic bubble oscillation. In order to determine the behaviour at finite λ, it is necessary to make an additional assumption so as to obtain a tractable problem. Equation (4.4) simplifies if we make a supposition

regarding the size of volume oscillations. The analysis that follows in this section is therefore further restricted to small oscillations about the mean volume.

Under this assumption, the volume of the bubble, which is proportional to $x^3(\tau)$, can be split into a mean and an oscillating part

$$x^3(\tau) \equiv V_0 + \Delta(\tau), \qquad V_0 = \langle x^3(\tau)\rangle_\tau, \ \langle \Delta(\tau)\rangle_\tau = 0, \ |\Delta(\tau)| \ll 1.$$

Using the binomial theorem, the average within (2.12) may be expanded to yield

$$\langle (3\sigma + x^3(\tau))^{(4/3)} \rangle_\tau$$
$$= (3\sigma + V_0)^{(4/3)} \left(1 + \frac{\frac{4}{3}\left(\frac{4}{3}-1\right)}{2!} \frac{\langle \Delta^2(\tau)\rangle_\tau}{(3\sigma+V_0)^2} + \frac{\frac{4}{3}\left(\frac{4}{3}-1\right)\left(\frac{4}{3}-2\right)}{3!} \frac{\langle \Delta^3(\tau)\rangle_\tau}{(3\sigma+V_0)^3} + \cdots \right).$$

The mean values of the various powers of $\Delta(\tau)$ are identified as the central moments. The first central moment, of course, is zero. For an arbitrary nonlinear bubble oscillation, it is impossible to know *a priori* which of the central moments is most significant. We will therefore combine the remaining terms of the expansion into a single function,

$$\delta\, f(\sigma) \equiv \frac{\frac{4}{3}\left(\frac{4}{3}-1\right)}{2!} \frac{\langle \Delta^2(\tau)\rangle_\tau}{(3\sigma+V_0)^2} + \frac{\frac{4}{3}\left(\frac{4}{3}-1\right)\left(\frac{4}{3}-2\right)}{3!} \frac{\langle \Delta^3(\tau)\rangle_\tau}{(3\sigma+V_0)^3} + \cdots,$$

where δ is a small parameter associated with the bubble oscillation defined by the latter equation and $f(0) = 1$. Furthermore, (2.12) can be brought to a well-known form by the variable transformations

$$C^0_{sm}(\sigma,\lambda) = \frac{n(\sigma,\lambda)}{(3\sigma+V_0)^{(1/3)}} = \frac{n(\sigma,\lambda)}{z + V_0^{(1/3)}},$$
$$z = (3\sigma + V_0)^{(1/3)} - V_0^{(1/3)}.$$

This leads to

$$\frac{\partial n}{\partial \lambda} = \frac{\partial^2 n}{\partial z^2} + \frac{\delta}{z + V_0^{(1/3)}} \frac{\partial}{\partial z}\left[f(z) \left((z + V_0^{(1/3)}) \frac{\partial n}{\partial z} - n \right) \right],$$

with boundary and initial conditions

$$n(z = 0, \lambda,) = V_0^{(1/3)} \left[C_{sb}\, \langle p^*_G(\tau)\rangle_{\hat{\tau}} - C_\infty \right],$$
$$n(z, \lambda = 0) = n(z \to \infty, \lambda) = 0.$$

This may be solved using a regular perturbation in the small parameter δ, of the form

$$n(z,\lambda) = n^0(z,\lambda) + \delta\, n^1(z,\lambda) + \cdots.$$

The zeroth-order problem is given by

$$\frac{\partial n^0}{\partial \lambda} = \frac{\partial^2 n^0}{\partial z^2},$$
$$n^0(z = 0, \lambda,) = V_0^{(1/3)} \left[C_{sb}\, \langle p^*_G(\tau)\rangle_{\hat{\tau}} - C_\infty \right],$$
$$n^0(z, \lambda = 0) = n^0(z \to \infty, \lambda) = 0,$$

and can be solved by Laplace transforms in λ, to yield

$$n^0 = V_0^{(1/3)} \left[C_{sb}\, \langle p^*_G(\tau)\rangle_{\hat{\tau}} - C_\infty \right] \operatorname{erfc}\left[\frac{z}{2\lambda^{(1/2)}} \right].$$

The first-order problem in the small parameter δ is

$$\frac{\partial n^1}{\partial \lambda} - \frac{\partial^2 n^1}{\partial z^2} = \frac{\delta}{z + V_0^{(1/3)}} \frac{\partial}{\partial z}\left[f(z)\left((z + V_0^{(1/3)})\frac{\partial n^0}{\partial z} - n^0\right)\right] \equiv Y(z,\lambda)$$

with homogeneous boundary conditions. This problem is readily solved with the use of a Green's function (Carslaw & Jaeger 1959),

$$n^1(z,\lambda) = \int_0^{\lambda}\int_0^{\infty} Y(z',\lambda')\, G(z,z',\lambda-\lambda')\mathrm{d}z'\mathrm{d}\lambda',$$

where

$$G(z,z',\lambda) = \frac{1}{2(\pi\lambda)^{(1/2)}}\left(\exp\left[-\frac{(z-z')^2}{4\lambda}\right] - \exp\left[-\frac{(z+z')^2}{4\lambda}\right]\right).$$

The details are too long to be included here, but we do use this solution to compute the associated mass transport

$$\frac{\mathrm{d}m^*_{G_{sm}}(\lambda)}{\mathrm{d}\lambda} = -3\langle x^4(\tau)\rangle_\tau\, V_0^{(1/3)}\, \left[C_{sb}\,\langle p^*_G(\tau)\rangle_{\hat{\tau}} - C_\infty\right]\left\{\frac{1}{V_0(\pi\lambda)^{(1/2)}} + \frac{1}{V_0^{(4/3)}}\right.$$
$$\left. + \frac{\delta}{V_0}\int_0^{\infty}\left(\dot{f}(z')\frac{\exp\left[-z'^2/\lambda\right]}{(\pi\lambda)^{(1/2)}} + \dot{f}(z')\frac{\mathrm{erfc}\left[z'/\lambda\right]}{(z'+V_0^{(1/3)})} - f(z')\frac{z'\exp\left[-z'^2/\lambda\right]}{(\pi\lambda^3)^{(1/2)}}\right)\mathrm{d}z'\right\}.$$

For the numerically computed bubble oscillations reported above, we found that the asymptotic form (4.6) is reached by $\lambda \approx 10$.

Appendix C. Comparison between non-polytropic and polytropic bubble models

Finally, we turn to the influence of the bubble dynamical model itself on the threshold pressure amplitudes and bubble growth rates that one calculates for nonlinear bubble oscillations. The vast majority of studies of rectified diffusion have made use of a polytropic expression for the bubble internal pressure. There is one exception of which we are aware – the numerical study of Kamath & Prosperetti (1990). In the results we presented above, we made use of the non-polytropic expression for the bubble internal pressure due to Kamath & Prosperetti (1989). As we show in what follows, the primary difference in the results for the polytropic model is a large increase in the effect of resonance. It appears that resonances are of lesser importance in the non-polytropic model owing to the greater care with which the model accounts for thermal dissipation of energy.

To see this, we shall recreate figures 3 and 5, and an expanded version of figure 6, but with a polytropic bubble model for the purposes of comparison. We choose here to use a modification due to Prosperetti (1984) of the formulation of Keller & Miksis (1980). This formulation accounts for compressibility of the liquid; for thermal, viscous and radiation damping; and makes use of the theoretically estimated polytropic exponent (η) of Prosperetti (1984). The formulation compares well with more sophisticated models in a recent careful study by Gaitan *et al.* (1992).

The governing equations for the bubble sub-system are the same as in the non-polytropic case. The dimensionless bubble internal pressure however, is assumed to

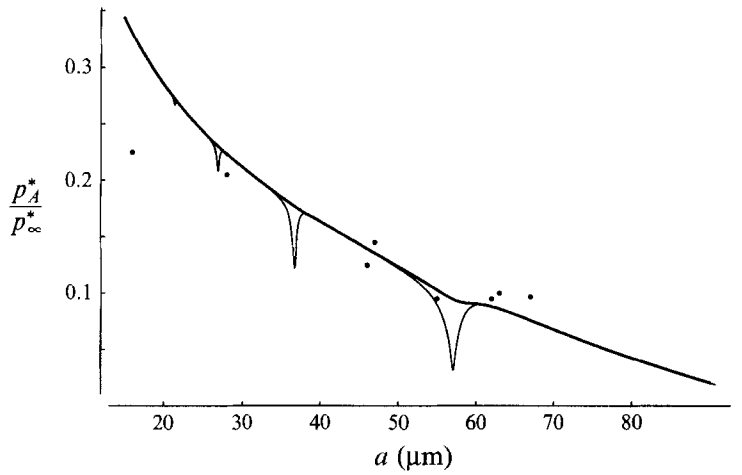

FIGURE 8. A plot of the ratio of the threshold pressure amplitude for rectified diffusion to the steady part of the background pressure versus equilibrium bubble radius. This is a comparison between the non-polytropic bubble model (heavy curve) and a polytropic bubble model (fine curve). The heavy curve corresponds to the dashed curve of figure 3. The bubbles are driven at a frequency of 26.6 kHz, the liquid saturation is 101.5 % and the interfacial tension is 73 dynes cm^{-1}.

have the following form

$$p_G^*(\tau) = \frac{1}{x^{3\eta}(\tau)},$$

which provides an alternative for the energy equation.

Continuation is again used as the basic technique for developing numerical solutions to the bubble dynamical equations, and for testing the threshold criterion. In figure 8, we show the threshold curves corresponding to the two bubble models for the previously examined case of figure 3. The threshold curves in figure 8 are comparable over the majority of the range in a. However, there are several dips in the fine curve corresponding to the polytropic bubble model. These are dips of variable magnitude, at which the threshold pressure decreases rapidly, and then rises again to nearly the same magnitude. The dips correspond to particularly efficient forcing of the (polytropic) bubble dynamics that occurs near a resonance between some natural frequency of the bubble and the forcing frequency. If one examines, for example, the maximum bubble radius over a period of oscillation versus the equilibrium bubble radius, then one observes clearly a jump in maximum bubble radius near these resonant dips in the polytropic bubble model. Clearly, while still present, the effects of resonances in the non-polytropic bubble model are much less.

A second example of the exaggerated importance ascribed to resonance in the polytropic bubble model can be seen in figure 9. Again we see various large jumps in bubble growth rate, which correspond to resonances of the system by comparison of figures 9 and 10. Where the fine curve in figure 9 is broken, the corresponding bubble oscillation is unstable, as determined by the moduli of the associated eigenvalues of the Poincaré map, computed by AUTO. The non-polytropic bubble model displays only a weak bump at resonance. It is clear that the more sophisticated bubble model would seem to eliminate unusual bubble growth rates near resonances as an explanation of the failure of the theory as it now stands to explain the disagreement of experimental results.

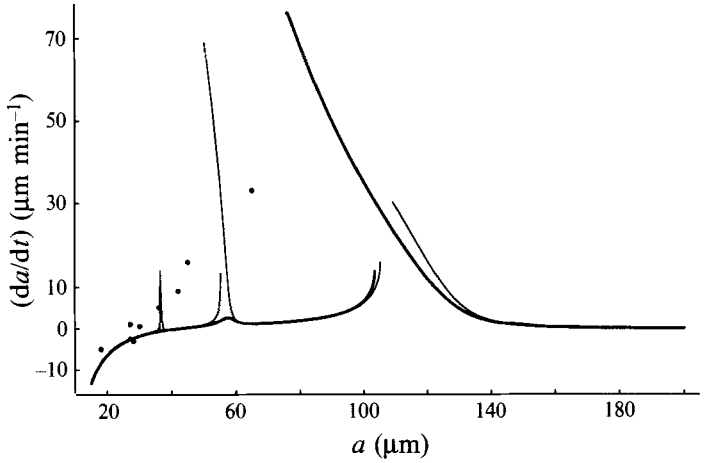

FIGURE 9. The rate of bubble growth in μm per minute versus equilibrium bubble radius in μm. This is a comparison between the non-polytropic bubble model (heavy curve) and a polytropic bubble model (fine curve). The bubbles are forced at a pressure amplitude of 0.2 bar. The curves correspond to (6.1), the points correspond to the experimental data of Eller (1969). The diffusivity of the gas in the liquid is 2.0×10^{-5} cm^2 s^{-1}. The bubbles are driven at a frequency of 26.6 kHz, and the interfacial tension is 73 dynes cm^{-1}.

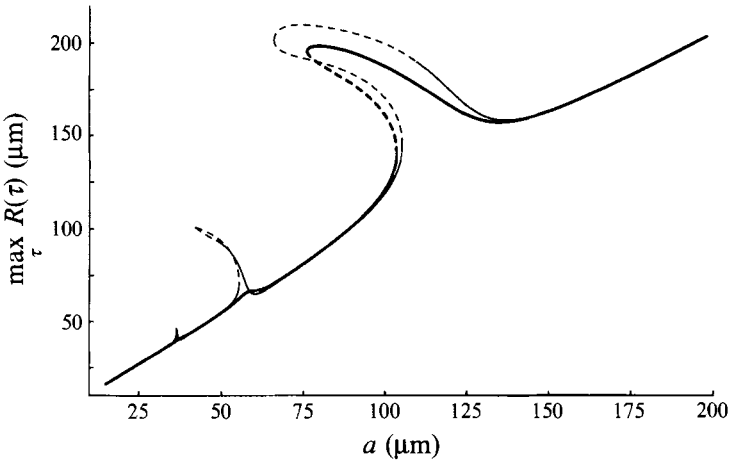

FIGURE 10. An expanded view of the bifurcation diagram of figure 6. This is a comparison between the non-polytropic bubble model (heavy curve) and a polytropic bubble model (fine curve). On the vertical axis, as a measure of the solution, we take the maximum bubble radius in μm over the period of oscillation. On the horizontal axis is the equilibrium bubble radius. The solid curves indicate stable bubble oscillations; unstable parts of the branch are shown as dashed curves. The bubbles are driven at a frequency of 26.6 kHz, the liquid is saturated and the interfacial tension is 73 dynes cm^{-1}.

As a third example of the very different behaviour of the two bubble models near resonance, we show a bifurcation diagram in figure 10 which is essentially a reproduction of figure 6 over a broader parameter range. Note that where there are multiple periodic solutions at the same parameter value, the maxima in the curves $R(\tau)$ (which are taken as the measures of the solutions) may occur at different τ. Where the curve is dashed, the corresponding bubble oscillation is unstable; where it

is solid, the bubble oscillation is stable. Although it is not possible to see in figure 10, there are two small folds for the polytropic response (fine curve) near 27 and 36μm, where the branch which comes from the left has a limit point where it reverses direction and becomes unstable, followed very quickly by another limit point where the branch again becomes stable. Hence there is a tiny range of parameters near 27 and 36μm where there are multiple stable attracting periodic bubble oscillations for the same forcing pressure amplitude in the polytropic model. Moreover, both stable branches can be reached by exploiting hysteresis in the standard way.

These remarks are perhaps more clear when one looks at the region around 52μm on the polytropic branch. There is an obvious limit point at 55.3μm where the polytropic branch doubles back and becomes unstable. Following this unstable portion of the branch, the solution develops very deep cusps that become increasingly difficult to compute. However, AUTO is able to track the cusps and follow the solutions. Continuing on the same branch, there is a bifurcation to an invariant torus (i.e. a secondary Hopf bifurcation of the associated fixed point of the Poincaré map that corresponds to quasi-periodic motion), where the periodic branch for the polytropic model becomes stable again when the radius is 50.2μm. The important feature to which we wish to draw attention is the rather large overlap, where there are two stable attracting periodic bubble oscillations for the polytropic model. Similar features were described by Lauterborn (1976), although his method of integrating through the transients makes it impossible to find unstable solutions or to determine bifurcations or to deduce the overall structure of the solution set. Either attractor may be reached by continuation from below or from above; hence there is hysteresis. Because the two attractors for the polytropic model in the parameter range 50.2–55.3μm are characterized by bubble oscillations of different shape and magnitude, the growth rates of bubbles following these two attractors are different (figure 9). In stark contrast, the corresponding resonance in the non-polytropic bubble model appears in the response curve as a small bump.

Finally, in figure 10, note the large fold that occurs near 105μm in both the polytropic and non-polytropic bubble models. The oscillations are unstable on the reversed part of the branches. In the non-polytropic model (heavy curve), the oscillations stabilize after a second limit point. In the polytropic model (fine curve), the oscillations stabilize after a bifurcation to an invariant torus near 110μm. For the polytropic model, this largest fold is similar to the one near 50μm, except that instead of a set of equilibrium bubble radii with multiple attracting periodic bubble oscillations, there is now a window of equilibrium bubble radii with no attracting periodic bubble oscillation. The dynamics in this window are most likely characterized by a quasi-periodic attractor corresponding to the invariant torus. Alternatively, the dynamics may be chaotic. In either case, we did not pursue intense study of the oscillations of larger bubbles, as Crum (1980) has reported that such bubbles are susceptible to visible surface waves upon excitation by the acoustic sound field; this behaviour violates the assumption of spherically symmetric motion we made at the outset. In addition, we note that the amplitude coefficients of the Galerkin expansion of the non-polytropic model decay only slowly for a greater than about 100μm. This indicates that some scepticism is in order regarding the results in this parameter range. Increasing the Galerkin approximation to more than four terms would be appropriate for further study.

These comparisons indicate that great care must be taken in studies of rectified diffusion to use an appropriate bubble model, particularly near resonances of the bubble dynamical equations.

REFERENCES

BLAKE, F. G. 1949 The onset of cavitation in liquids. I. Cavitation threshold sound pressures in water as a function of temperature and hydrostatic pressure. *Harvard University Acoustic Research Laboratory Technical Memorandum* 12, pp.1-52.

CARSLAW, H. S. & JAEGER, J. C. 1959 *Conduction of Heat in Solids*, Oxford University Press.

CHURCH, C. C. 1988 Prediction of rectified diffusion during nonlinear bubble pulsations at biomedical frequencies. *J. Acoust. Soc. Am.* **83**, 2210–2217.

CRUM, L. A. 1980 Measurements of the growth of air bubbles by rectified diffusion. *J. Acoust. Soc. Am.* **68**, 203–211.

CRUM, L. A. 1984 Acoustic cavitation series part five - Rectified diffusion. *Ultrasonics* **22**, 215–223.

CRUM, L. A. & HANSEN, G. M. 1982 Generalized equations for rectified diffusion. *J. Acoust. Soc. Am.* **72**, 1586–1592.

DOEDEL, E. A. 1986 AUTO: software for continuation and bifurcation problems in ordinary differential equations. California Institute of Technology Applied Mathematics Preprint.

ELLER, A. 1969 Growth of bubbles by rectified diffusion. *J. Acoust. Soc. Am.* **46**, 1246–1250.

ELLER, A. 1972 Bubble growth by diffusion in an 11-kHz sound field. *J. Acoust. Soc. Am.* **52**, 1447–1449.

ELLER, A. & FLYNN, H. G. 1965 Rectified diffusion during nonlinear pulsations of cavitation bubbles. *J. Acoust. Soc. Am.* **37**, 493–503.

FANNJIANG, A. & PAPANICOLAOU, G. 1994 Convection enhanced diffusion for periodic flows. *SIAM J. Appl. Maths* **54**, 333–408.

GAITAN, D. F., CRUM, L. A., CHURCH, C. C. & ROY, R. A. 1992 Sonoluminescence and bubble dynamics for a single stable cavitation bubble. *J. Acoust. Soc. Am.* **91**, 3166–3183.

HINCH, E. J. 1991 *Perturbation Methods*. Cambridge University Press.

HSIEH, D.-Y. & PLESSET, M. S. 1961 Theory of rectified diffusion of mass into gas bubbles. *J. Acoust. Soc. Am.* **33**, 206–215.

KAMATH, V. & PROSPERETTI, A. 1989 Numerical integration methods in gas-bubble dynamics. *J. Acoust. Soc. Am.* **85**, 1538–1548.

KAMATH, V. & PROSPERETTI, A. 1990 Mass transfer during bubble oscillations. In *Frontiers of Nonlinear Acoustics: Proceedings of the Twelfth Intl. Symp. on Nonlinear Acoustics* (ed. M. F. Hamilton & D. T. Blackstock), pp. 503–508. Elsevier.

KELLER, J. B. & MIKSIS, M. 1980 Bubble oscillations of large amplitude. *J. Acoust. Soc. Am.* **68**, 628–633.

KUNDU, J. P. 1990 *Fluid Mechanics*. Academic Press.

LAUTERBORN, W. 1976 Numerical investigation of nonlinear oscillations of gas bubbles in liquids. *J. Acoust. Soc. Am.* **59**, 283–293.

LEAL, L. G. 1992 *Laminar Flow and Convective Transport Processes: Scaling Principles and Asymptotic Analysis*. Butterworth-Heinemann.

NAGIEV, F. B. & KHABEEV, N. S. 1985 Dynamics of soluble gas bubbles. *Izv. Akad. Nauk SSSR, Mekh. Zhid. i Gaza* **6**, 52–59.

PLESSET, M. S. & PROSPERETTI, A. 1977 Bubble dynamics and cavitation. *Ann. Rev. Fluid Mech.* **9**, 145–185.

PLESSET, M. S. & ZWICK, S. A. 1952 A nonsteady heat diffusion problem with spherical symmetry. *J. Appl. Phys.* **23**, 95–98.

PROSPERETTI, A. 1984 Acoustic cavitation series part two – Bubble phenomena in sound fields: part one. *Ultrasonics* **22**, 69–77.

SKINNER, L. A. 1970 Pressure threshold for acoustic cavitation. *J. Acoust. Soc. Am.* **47**, 327–331.

SKINNER, L. A. 1972 Acoustically induced gas bubble growth. *J. Acoust. Soc. Am.* **51**, 378–382.

SMEREKA, P., BIRNIR, B. & BANERJEE, S. 1987 Regular and chaotic bubble oscillations in periodically driven pressure fields. *Phys. Fluids* **30**, 3342–3350.

STOKES, G. G. 1851 On the effect of the internal friction of fluids on the motion of pendulums. *Trans. Camb. Phil. Soc.* **9**, 8–106.

SZERI, A. J. & LEAL, L. G. 1991 The onset of chaotic oscillations and rapid growth of a spherical bubble at subcritical conditions in an incompressible liquid. *Phys. Fluids* A **3**, 551–555.